ACS APPLIED MATERIALS & INTERFACES

Research Article

www.acsami.org

Preparation and Characterization of Magnetic Porous Carbon Microspheres for Removal of Methylene Blue by a Heterogeneous Fenton Reaction

Lincheng Zhou,*[,†] Yanming Shao,[†] Junrui Liu,[†] Zhengfang Ye,[‡] He Zhang,[†] Junjun Ma,[†] Yan Jia,[†] Weijie Gao,[†] and Yanfeng Li[†]

[†]State Key Laboratory of Applied Organic Chemistry, College of Chemistry and Chemical Engineering, Institute of Biochemical Engineering & Environmental Technology, Lanzhou University, Lanzhou 730000, P. R. China

[‡]Department of Environmental Engineering, Key Laboratory of Water and Sediment Sciences of the Ministry of Education, Peking University, Beijing 100871, P. R. China

Supporting Information

ABSTRACT: High-specific-surface-area magnetic porous carbon microspheres (MPCMSs) were fabricated by annealing Fe^{2+}-treated porous polystyrene (PS) microspheres, which were prepared using a two-step seed emulsion polymerization process. The resulting porous microspheres were then sulfonated, and Fe^{2+} was loaded by ion exchange, followed by annealing at 250 °C for 1 h under an ambient atmosphere to obtain the PS-250 composite. The MPCMS-500 and MPCMS-800 composites were obtained by annealing PS-250 at 500 and 800 °C for 1 h, respectively. The iron oxide in MPCMS-500 mainly existed in the form of Fe_3O_4, which was concluded by characterization. The MPCMS-500 carbon microspheres were used as catalysts in heterogeneous Fenton reactions to remove methylene blue (MB) from wastewater with the help of H_2O_2 and NH_2OH. The results indicated that this catalytic system has a good performance in terms of removal of MB; it could remove 40 mg L^{-1} of MB within 40 min. After the reaction, the catalyst was conveniently separated from the media within several seconds using an external magnetic field, and the catalytic activity was still viable even after 10 removal cycles. The good catalytic performance of the composites could be attributed to synergy between the functions of the porous carbon support and the Fe_3O_4 nanoparticles embedded in the carrier. This work indicates that porous carbon spheres provide good support for the development of a highly efficient heterogeneous Fenton catalyst useful for environmental pollution cleanup.

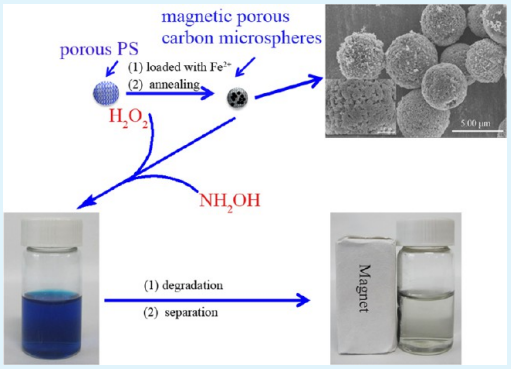

KEYWORDS: *carbon microspheres, magnetic, porous, heterogeneous, Fenton reaction, degradation, methylene blue*

1. INTRODUCTION

Advanced oxidation processes (AOPs) are potential alternative treatments for industrial wastewater containing nonbiodegradable organic pollutants. These involve the generation of a free hydroxyl radical (•OH), which degrades most organic pollutants quickly and nonselectively. The Fenton reaction is a well-studied AOP that uses hydrogen peroxide as an oxidant in the presence of a catalyst.[1−3] The nonselective attack of organic compounds by the hydroxyl radicals results in mineral end products. The classical Fenton reagent consists of a homogeneous solution of iron ions and hydrogen peroxide. Catalysis is effective only within a low and narrow pH range. It also produces iron sludge as a byproduct of the treatment, which is an additional environmental contaminant. Therefore, heterogeneous catalysts have been developed to overcome these problems.[4−7] The Fe^{2+} ion in Fe_3O_4 makes this a very efficient catalyst for the degradation of organic compounds and also allows it to be easily separated from the reaction medium using an external magnetic field. Therefore, magnetite is suitable as a heterogeneous Fenton catalyst.

However, Fe_3O_4 nanoparticles usually form aggregates during the reaction process, leading to reduced catalytic activity.[8] So, significant effort has been made to improve this situation.[3,9−11] Iron oxides can be immobilized on organic or inorganic supports to form novel heterogeneous Fenton catalysts. Carbon materials such as multiwalled carbon nanotubes,[4,10] graphene,[12,13] and activated carbon[14,15] have attracted great attention because of their excellent properties, including high thermal stability and acid/base resistance. Supports that possess high specific surface area can improve the activity of iron oxide by preventing aggregation of the catalyst and improving its dispersibility.[16] Porous carbon microspheres not only have the advantages of the carbon

Received: January 26, 2014
Accepted: April 14, 2014
Published: April 14, 2014

materials mentioned above but also possess high specific surface area, making them ideal candidates for heterogeneous Fenton catalyst support. Annealing polymer spheres with an iron source can fabricate magnetic porous carbon spheres.[17−21] Margel et al. reported the use of $FeCl_2$,[17] ferrocene,[18,20] and $Fe(CO)_5$[19] as sources of iron, and porous poly(divinylbenzene) (PDVB) spheres as a source of carbon, to fabricate magnetic porous carbon spheres. The resulting hybrid particles possessed good spherical morphology, but the use of toxic compounds such as $Fe(CO)_5$ was a drawback to this approach. However, the high degree of cross-linking and stability allowed PDVB to retain its complete skeleton, which led to reduced surface areas in these hybrids after annealing, compared with the original porous polymer spheres. Liu and Yan[21] reported the preparation of magnetic carbon spheres by annealing acrylic acid and divinylbenzene (DVB) copolymer microspheres, with uptake of the Fe^{2+} ions achieved through ion exchange. However, the specific surface area of these magnetic hybrids was low because of the spheres' initial lack of pores.

In the present work, high-specific-surface-area magnetic porous carbon microspheres (MPCMSs) were prepared by annealing porous polystyrene (PS) microspheres that had been sulfonated and loaded with Fe^{2+} by ion exchange. The magnetic porous microspheres were then characterized using scanning electron microscopy (SEM), X-ray diffraction (XRD), Mössbauer spectroscopy (MS), Raman spectroscopy, Fourier transform infrared (FT-IR) spectroscopy, vibrating sample magnetometry, and Brunauer−Emmett−Teller (BET) analyses. The ability of the particles to facilitate the Fenton oxidation of methylene blue (MB) was tested under varying conditions of initial pH, H_2O_2 concentration, catalyst dosage, and NH_2OH concentration. The stability and reusability of the magnetic porous carbon spheres were also tested.

2. EXPERIMENTAL SECTION

2.1. Materials. Styrene (Shantou Xilong Chemical Co. Ltd) was initially washed with a 1 mol L^{-1} NaOH solution to remove the inhibitor and then purified by vacuum distillation. DVB (80%, Aldrich) was purified by passing it through activated aluminum oxide to remove any inhibitor. Poly(vinylpyrrolidone) (PVP K-30; M_w = 40000 g mol^{-1}) was obtained from Shanghai Sitong Reagent Co. Ltd. (China). Sodium dodecyl sulfate (SDS), 2,2-azobis(isobutyronitrile) (AIBN), benzoyl peroxide (BPO), hydrogen peroxide, and dibutyl phthalate (DBP) were supplied by Tianjin Guangfu Fine Chemical Research Institute. AIBN and BPO were purified by recrystallization. Hydroxyethyl cellulose (HEC) was supplied by Xuanguang Chemical Technology Co. Ltd. MB was obtained from Tianjin Tiantai Fine Chemicals Co., Ltd. Hydroxylamine hydrochloride was supplied by Sinopharm Chemical Reagent Co., Ltd. All other chemicals were of analytical grade and were used without any further purification.

2.2. Preparation of Seed Particles by Dispersion Polymerization. The monodisperse PS seed particles were fabricated by dispersion polymerization methods in an ethanol medium with PVP K-30 as a stabilizer and AIBN as an initiator. In a typical experiment, 100 mL of ethanol and 1 g of PVP were added into a four-necked round-bottom flask, which was equipped with a mechanical stirrer, followed by stirring into a homogeneous phase and purging with nitrogen for 30 min. After the temperature was elevated to 74 °C, 25 mL of styrene and 0.2 g of AIBN were added into the reactor, and polymerization was allowed to continue at 120 rpm for 24 h. The PS spheres were obtained by centrifugation and repeatedly washed with ethanol to remove residual styrene and PVP. Thereafter, the beads were dried under a vacuum at ambient temperature.

2.3. Preparation of Porous Microspheres by a Two-Step Seed Emulsion Polymerization. The seed particles (1 g) were redispersed in 100 mL of a 0.25% SDS aqueous solution by magnetic stirring, followed by the addition of 1 mL of DBP into the flask. The mixture was redispersed by sonication for 30 min, and then the mixture was stirred for 10 h at 35 °C. The mixture of styrene (10 g), DVB (1 g), toluene (15 mL), and BPO (0.1 g) was poured into the reactor, which had been emulsified with 100 mL of a 0.25% SDS solution by sonication for 30 min. The swelling stage of the monomer was held for another 10 h at 35 °C. Finally, 50 mL of a 1 wt % HEC aqueous solution was added into the reactor. Thereafter, polymerization was carried out at 80 °C for 24 h. The beads were obtained by repeated centrifugation, followed by washing three times with ethanol. The cleaned beads were dried under a vacuum at 30 °C, followed by extraction with toluene to remove linear PS and porogen. The resulting microspheres were washed with acetone and dried under a vacuum.

2.4. Sulfonation of Porous Microspheres. The porous PS microspheres (1 g) were placed in a 50 mL round-bottomed flask, then 96% H_2SO_4 (4 g) and Ag_2SO_4 (12.5 mg) were added, and the mixture was refluxed at 80 °C for 2 h. After sulfonation, the microspheres were washed five times with distilled water and vacuum-dried at 40 °C for 24 h. The sulfonated microspheres were labeled as PS-SO_3H.

2.5. Preparation of Porous Magnetic Carbon Spheres. The PS-SO_3H microspheres (1 g) were transferred into a 250 mL three-necked round-bottom flask, and then 100 mL of a 0.5 mol L^{-1} $FeCl_2$ solution was added into the flask and stirred overnight under a nitrogen atmosphere. After that, the microspheres were separated by centrifugation and washed with deionized water until no Fe^{2+} remained, as determined using a KSCN solution. The microspheres were then dried under a vacuum at 40 °C, followed by annealing at 250 °C for 1 h under an ambient atmosphere to obtain the PS-250 composite. The PS-250 composite was then annealed at either 500 or 800 °C for 1 h under inert atmospheric conditions to synthesize MPCMS-500 or MPCMS-800, respectively.

2.6. Dye Decoloration through a Heterogeneous Fenton Reaction. A degradation experiment was carried out by which the carbon sphere was added into 10 mL of a 40 mg L^{-1} MB solution in the presence of H_2O_2 and NH_2OH, and the suspension was shaken in a thermostated shaker at 120 rpm at 30 °C. After the reaction, the carbon spheres were separated using an external magnetic field, and the concentration of MB was determined using a UV−vis spectrometer, with a maximum absorbance wavelength for MB at 664 nm. Total organic carbon (TOC) was determined by a TOC analyzer after filtration through a 0.45 μm membrane filter.

2.7. Characterization. FT-IR spectra were obtained in transmission mode on a FT-IR spectrometer (American Nicolet Corp. model 170-SX) using the KBr pellet technique. Thermogravimetric analysis (TGA) and differential scanning calorimetry (DSC) were performed on a STA PT1600 system in a nitrogen atmosphere with a heating rate of 20 °C min^{-1} in the temperature range of 30−1000 °C. XRD [Rigaku D/MAX-2400 X-ray diffractometer with Ni-filtered Cu Kα radiation (λ = 1.54056)] was used to investigate the crystal structure of the nanoparticles. MS studies were performed using a conventional constant-acceleration drive and a 50 m Ci ^{57}Co:Rh source. The velocity calibration at room temperature (RT) was performed using an α-Fe absorber, and the isomer shift (IS) values reported are relative to α-Fe. Raman spectra were recorded on a Dilor LABRAM-1B multichannel confocal microspectrometer. The surface morphology was characterized with an FEI SEM model Inspect S. The iron content of the sample obtained by microwave-digested samples and the iron concentration were determined using inductively coupled plasma (ICP). Magnetization measurements at RT were obtained using a vibrating sample magnetometer (Lake Shore model 7304, Westerville, OH) at RT. X-ray photoelectron spectroscopy (XPS) spectra were obtained with an ESCALab220i-XL electron spectrometer (VG Scientific) using 300 W Al Kα radiation The N_2 adsorption−desorption isotherm was measured at liquid-nitrogen temperature (77 K) using a Micromeritics ASAP 2020 analyzer. The specific surface area was calculated by the BET method. The pore-size distribution was obtained using the Barrett−Joyner−Halenda (BJH) method. UV−vis detection was carried out on a TU-1810PC UV−vis spectrophotometer (Purkinje General, Beijing, China). All fluorescence spectra

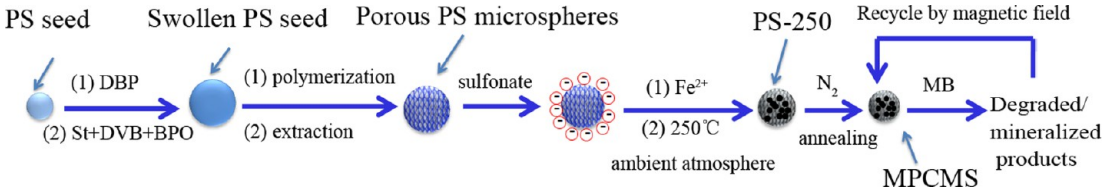

Figure 1. Schematic illustration of the synthesis process used to fabricate MPCMSs.

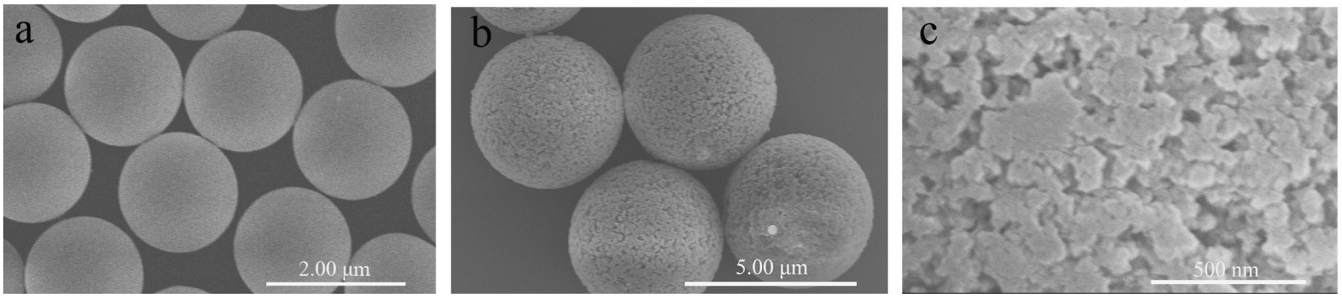

Figure 2. SEM images of (a) PS seed spheres (×20000) and (b and c) porous PS microspheres (magnification: b, ×10000; c, ×90000).

were recorded using a F97Pro spectrofluorophotometer (LengGuang Industrial Co., Ltd., Shanghai, China). TOC was determined using a TOC analyzer (Elementar vario TOC cube, Hanau, Germany).

3. RESULTS AND DISCUSSION

3.1. Morphology and Structural Characterization. The porous PS microspheres were fabricated by seed emulsion polymerization.[22] Figure 1 outlines the steps required for the preparation of uniform MPCMS. First, uniform PS seed spheres were swelled in DBP and an emulsion containing monomeric styrene, the initiator BPO, and the cross-linker monomer DVB. Then, polymerization of styrene was carried out within the swollen PS seed spheres at 80 °C. Finally, uniform porous PS microspheres were obtained after dissolution of the PS seeds and toluene components of the original composite particles. The porous PS microspheres were then treated with concentrated sulfuric acid to form negative charged groups on their surfaces. Fe^{2+} uptake on the spheres was achieved through ion exchange. Subsequent annealing of these microspheres at 250 °C under ambient atmospheres resulted in the synthesis of PS-250. Samples MPCMS-500 and MPCMS-800 were obtained by annealing PS-250 under an inert atmosphere at 500 and 800 °C, respectively.

SEM images of the PS seed spheres (Figure 2a) and porous PS microspheres (Figure 2b,c) revealed that both the PS seed spheres and the porous PS microspheres were perfectly spherical with a narrow range of size distribution (Figure S1 in the Supporting Information, SI). The size and size distribution of these particles were 1.71 ± 0.04 and 4.4 ± 0.24 mm, respectively. The images also clearly illustrate the differences between the surfaces of the porous PS microspheres and the smooth original PS seed spheres.

FT-IR spectra of the porous PS microspheres and PS-SO_3H (Figure S2 in the SI) revealed styrene absorption bands at 700, 757, 1452, 1493, 1601, 2852, 2924, and 3026 cm^{-1}, as expected.[23] The peaks at 1176 cm^{-1} corresponded to the stretching vibration of the S═O in SO_3H,[24] which demonstrates successful sulfonation of the porous PS microspheres.

The thermal stability of the porous PS microspheres was studied by TGA and DSC under an inert atmosphere. Parts a and b of Figure 3 present typical TGA and DSC thermograms of the porous PS microspheres. The TGA curve exhibits a steep slope between 300 and 600 °C, indicating about 90% weight loss due to decomposition of the porous PS microspheres, leaving residual carbon. This observation is in good agreement with the DSC curve that exhibits an endothermic peak at approximately 420 °C, which was likely related to carbonization of the porous PS microspheres. TGA demonstrated the durability of the porous PS microspheres at an annealing temperature of 250 °C.

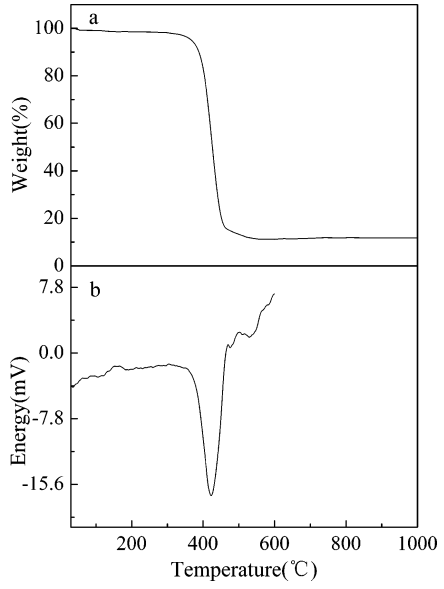

Figure 3. TGA (a) and DSC (b) thermograms of the porous PS microspheres.

Figure 4 shows the XRD patterns of the PS-250, MPCMS-500, and MPCMS-800 composite microspheres. PS-250 exhibited formation of α-Fe_2O_3 with a small fraction of a maghemite phase. The diffraction peaks were in good agreement with the standard values for α-Fe_2O_3 (JCPDS 33-0664).[25] The diffraction peaks of the composite annealed at 500 °C indicated Fe_3O_4 with a small fraction of α-Fe_2O_3, which were also in agreement with reported values (JCPDS 65-

dx.doi.org/10.1021/am500576p | ACS Appl. Mater. Interfaces 2014, 6, 7275−7285

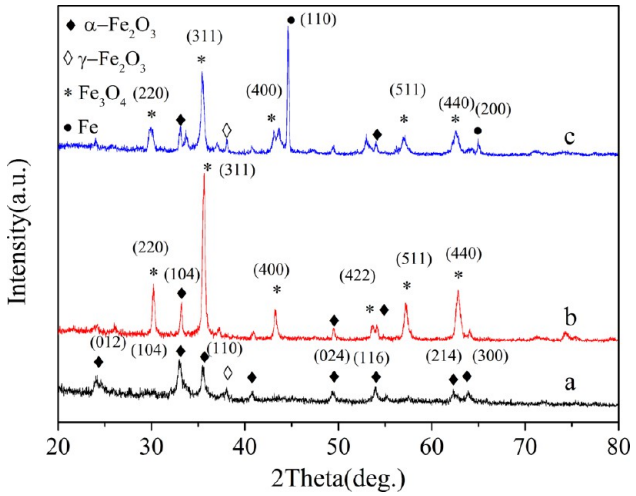

Figure 4. XRD patterns of (a) PS-250 (b) MPCMS-500, and (c) MPCMS-800.

3107).[26] The XRD pattern of the composite obtained at 800 °C indicated the formation of Fe_3O_4 and the iron phase.

It should be noted that the XRD patterns of magnetite (Fe_3O_4) and maghemite (γ-Fe_2O_3) are similar. Thus, MS at RT was employed to distinguish the components of these composites, as described below. The RT MS spectra of the PS-250, MPCMS-500, and MPCMS-800 composites can be seen in Figure 5. In Figure 5a, sextets with IS = 0.37 mm s^{-1}

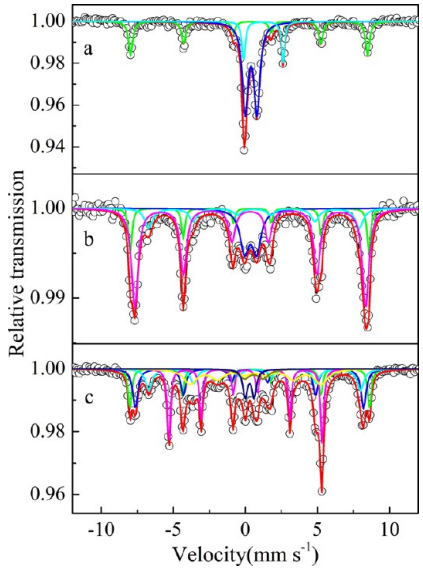

Figure 5. MS spectra at RT of (a) PS-250 (b) MPCMS-500, and (c) MPCMS-800.

and H_{eff} = 51.06 T are related to γ-Fe_2O_3 (29.7%).[17] The one doublet, which accounts for 55.6%, with IS = 0.39 mm s^{-1} and QS = 0.82 mm s^{-1} may be attributed to α-Fe_2O_3.[27] Another doublet (14.7%) with the parameters of IS = 1.24 mm s^{-1} and QS = 2.74 mm s^{-1} may be ascribed to Fe^{2+}, which did not totally oxidize in the preparation process of PS-250. In Figure 5b, the spectrum was interpreted by three sextets and one doublet. The sextet that accounts for 13.3% of the spectral area with IS = 0.38 mm s^{-1} and H_{eff} = 51.3 T is Fe_2O_3. The two other sextets (H_{eff} = 45.3 and 49.7 T and IS = 0.59 and 0.33 mm s^{-1}) belong to magnetite, which accounts for 70.5%. The doublet accounting for 16.2% with IS = 0.36 mm s^{-1} and QS = 0.84 mm s^{-1} may be nonmagnetic Fe_2O_3. The MS spectrum of MPCMS-800 is seen in Figure 5c; one sextet (IS = 0.37 mm s^{-1} and H_{eff} = 51.5 T), which accounts for 3.9%, can be ascribed to Fe_2O_3. The two additional sextets that account for 33.5% are related to Fe_3O_4 as described above. The sextet that accounts for 23% of the spectral area with H_{eff} = 33 T (IS = 0 mm s^{-1}) is the pure metallic iron. The extra doublet (IS = 0.59 mm s^{-1} and QS = 1.3 mm s^{-1}), which accounts for 4.9%, may be attributed to the nonmagnetic superparamagnetic nanoparticles of Fe_3O_4 above their blocking temperature. Another doublet, with IS = 0.3 mm s^{-1} and QS = 0.62 mm s^{-1} and accounting for 6.2%, can be ascribed to Fe_2O_3.

The Raman spectra of these three composites are displayed in Figure 6. Peaks at 225, 291, 408, 496, and 610 cm^{-1} for PS-

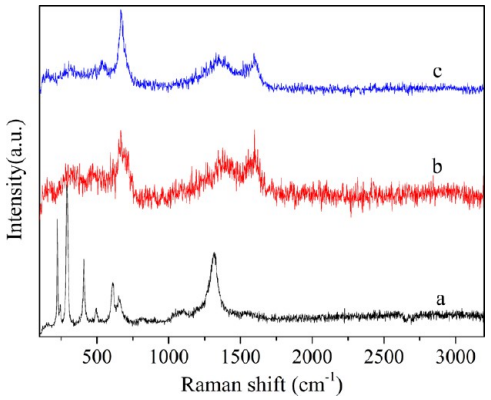

Figure 6. Raman spectra of (a) PS-250, (b) MPCMS-500, and (c) MPCMS-800.

250 were found to match with previously reported data for hematite.[27,28] The Raman spectra of both MPCMS-500 and MPCMS-800 clearly revealed the characteristic peaks of Fe_3O_4 at 302, 504, and 670 cm^{-1}, demonstrating the presence of Fe_3O_4 in these samples.[29,30] The D band at 1355 cm^{-1} and the G band at 1600 cm^{-1} exhibited similar intensities, indicating the amorphous carbon structure of these samples.[31]

FT-IR spectra of PS-250, MPCMS-500, and MPCMS-800 are summarized in Figure S3 in the SI. PS-250 exhibited peaks at 600 and 475 cm^{-1}, which were assigned to Fe−O characteristic vibrations from α-Fe_2O_3.[32] The peak at 568 cm^{-1} was ascribed to the Fe−O stretching vibration in Fe_3O_4.[33] These results indicated that Fe_3O_4 was present in both MPCMS-500 and MPCMS-800.

SEM images of samples PS-250, MPCMS-500, and MPCMS-800 (Figure 7) revealed that their constituent microspheres retained their spherical shapes; however, their diameters decreased gradually with increasing annealing temperature, which was likely caused by contraction of the microspheres during the hotter annealing step. The diameters observed in the three samples were 4.0 ± 0.12, 3.5 ± 0.33, and 3.2 ± 0.35 μm, respectively. High-magnification SEM micrographs of PS-250, MPCMS-500, and MPCMS-800 (Figure 7c,f,i) confirmed that the microspheres remained porous after annealing.

N_2 adsorption−desorption isotherms (Figure 8a) and pore-size-distribution curves (Figure 8b) of the three annealed samples revealed that the BET surface areas of the PS-250, MPCMS-500, and MPCMS-800 microspheres were 30.50, 362.52, and 386.69 m^2 g^{-1}, respectively. Detailed data for this are summarized in Table S1 in the SI. The specific surface area

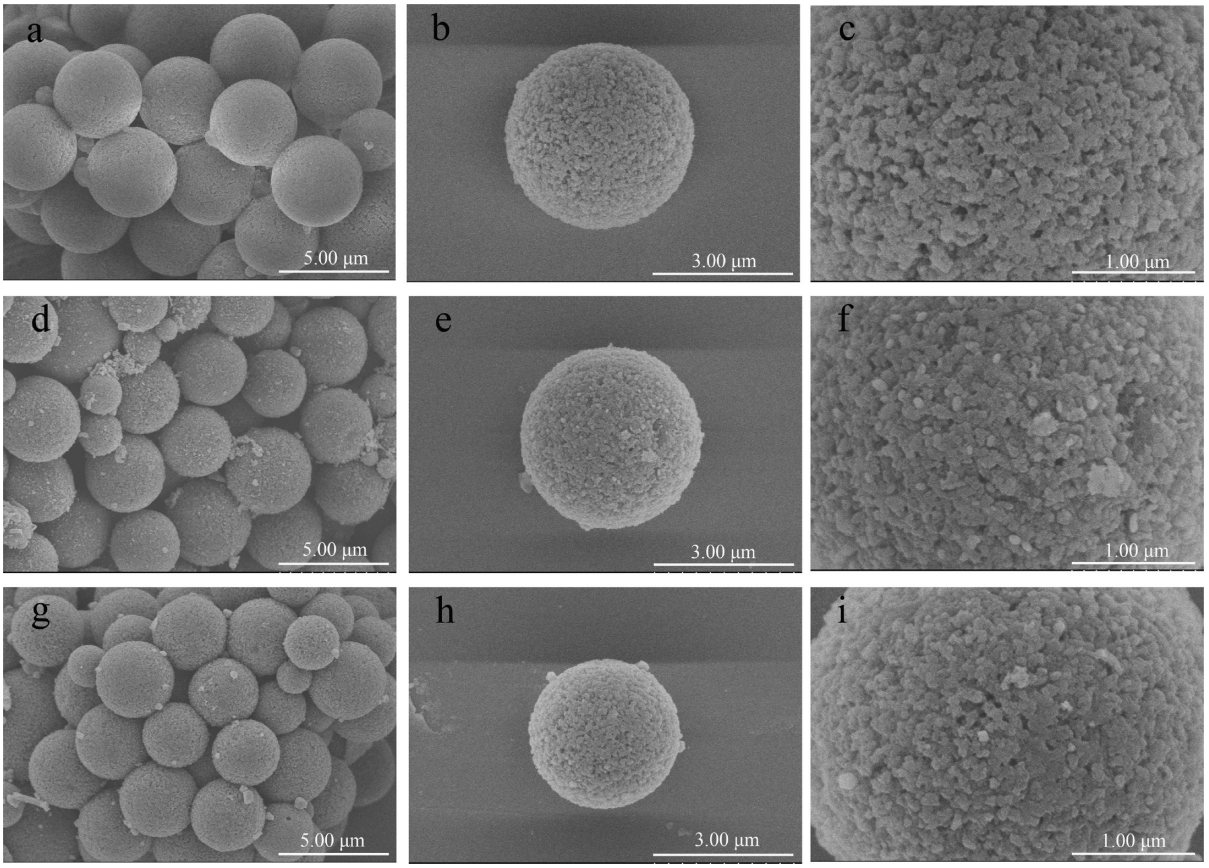

Figure 7. SEM images of (a–c) PS-250 (×7000), (d–f) MPCMS-500 (×15000), and (g–i) MPCMS-800 (×40000).

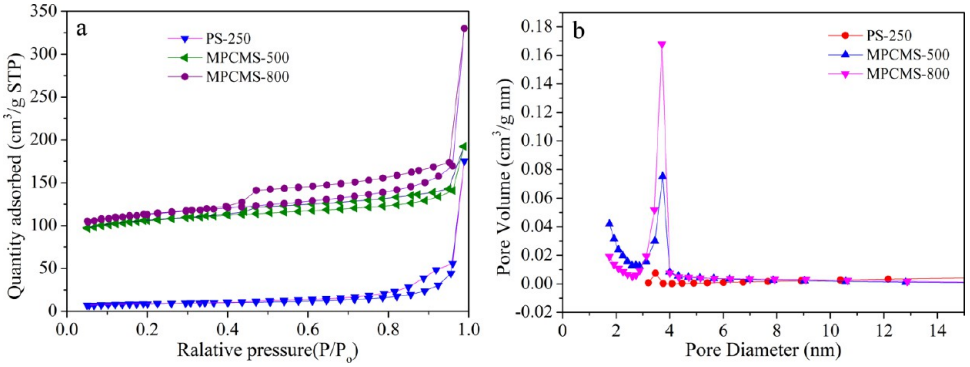

Figure 8. (a) N_2 adsorption–desorption isotherms and (b) the pore-size-distribution curve obtained from the desorption data through the BJH method.

appeared to increase with increasing annealing temperature. Each of the annealed samples exhibited higher values than those of the nonannealed porous PS microspheres. They also exhibited higher specific surface areas than magnetic carbon microspheres reported in previous studies using porous polymer microspheres as carbon precursors (Table S2 in the SI).[17−20] The increased BET surface area may have been caused by the decreased diameter and decomposition of some unstable substances, such as linear PS, that were not completely removed during the extraction process. Any residual linear PS would have acted as a porogen during annealing. The pore-size-distribution curves of the PS-250, MPCMS-500, and MPCMS-800 microspheres were estimated from the desorption curves of the isotherm using BJH analyses. The higher BET surface areas of the catalyst supports should be useful for pollutant removal by increasing the contact frequency between the pollutants and catalyst.

The magnetic properties of PS-250, MPCMS-500, and MPCMS-800 are depicted in Figure 9. Their saturation magnetizations are 3.2, 35.3, and 42.5 emu g^{-1}, respectively. Furthermore, PS-250 exhibits superparamagnetic behavior at RT with no coercivity and remanence. MPCMS-500 and MPCMS-800 indicated ferromagnetic-type curves, which show a hysteresis loop. The values of coercivity and remanence are summarized in Table 1. The content of iron for the three samples was also tested, and it increased with the annealing temperature (Table 1). The saturation magnetization values of MPCMS-500 and MPCMS-800 suggested that they could be easily separated by an external magnetic field (Figure S4 in the SI). The combination of high BET surface areas and sensitive

dx.doi.org/10.1021/am500576p | ACS Appl. Mater. Interfaces 2014, 6, 7275−7285

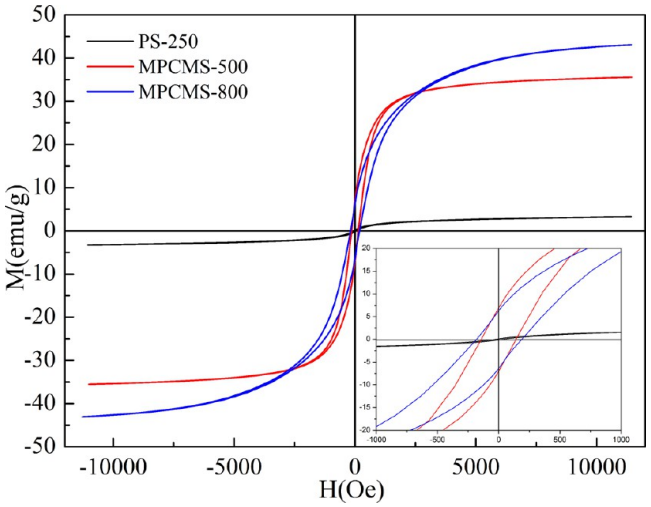

Figure 9. Magnetic hysteresis loops of PS-250, MPCMS-500, and MPCMS-800. The inset is a magnified view of the magnetization versus field curves.

Table 1. Magnetic Properties and Iron Content of PS-250, MPCMS-500, and MPCMS-800

		magnetic properties	
sample	Fe (wt %)	M_s (emu g^{-1})	H_c (Oe)
PS-250	23.5	3.2	
MPCMS-500	39.6	35.3	141.9
MPCMS-800	50.5	42.5	185.4

magnetic responses suggested that the obtained hybrid would be suitable as a catalyst support and adsorbent.

3.2. Catalytic Properties of Magnetic Porous Carbon Spheres. The formation of an iron phase in MPCMS-800 could lead to iron forming a primary battery with carbon, which would result in leakage of the iron ions during the heterogeneous Fenton reaction. Using ICP, MPCMS-800 was seen to produce a maximum ion leakage concentration of 500 mg L^{-1} during the heterogeneous Fenton reaction. Because of this, MPCMS-800 was not considered the best catalyst, and MPCMS-500 was subsequently selected for further analysis as a catalyst for MB degradation.

The ability of MPCMS-500 to remove MB was tested in different systems (Figure 10). Adding the carbon spheres to a MB solution alone led to almost 30% MB removal, which was likely due to adsorption only. Using MPCMS-500 in the presence of H_2O_2 and NH_2OH led to the removal of nearly all of the MB within 25 min. The degradation of MB was compared using pristine Fe_3O_4, which was prepared by traditional coprecipitation in an otherwise similar system with H_2O_2 and NH_2OH. Using similar dosages of the catalyst, MPCMS-500 performed much more efficiently than the unmodified Fe_3O_4. This suggests that the porous carbon support aided the degradation of MB through adsorption and thereby improved the reaction rate. Evidence from previous studies has indicated that synergy results from the adsorptive properties of the support, which increases the rate of substrate degradation. Similar effects were reported by Hu,[4] who observed that the degradation of pollutants, such as 17α-methyltestosterone, can be accelerated via their adsorption onto multiwalled carbon nanotubes and by Noorjahan,[34] who reported that zeolite supports positively affected the degradation of phenol. In the case of MB, the substrate molecules adsorbed near the immobilized iron oxide could be easily attacked by the generated $^{\bullet}OH$.

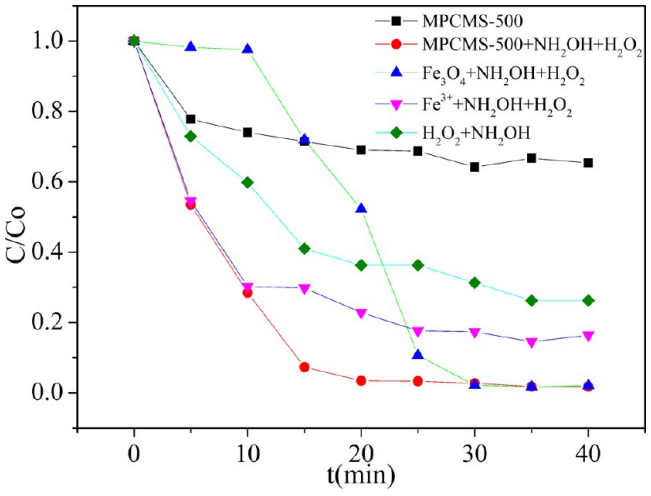

Figure 10. Removal efficiency of MB under different conditions within 40 min. Reaction conditions: initial MB concentration, 40 mg L^{-1}; initial H_2O_2 concentration, 16 mmol L^{-1}; NH_2OH concentration, 4 mmol L^{-1}; catalyst load, 2 g L^{-1}; initial solution pH, 5.0; T = 303 K.

Considering the efficiency of MB degradation, the composites exhibited more effective removal of MB than unmodified Fe_3O_4. A negligible number of iron ions can inevitably leach from the heterogeneous Fenton catalyst during the reaction process. To rule out the possibility that the observed catalytic activity was caused by the leached Fe^{3+}, the catalysts were removed by a magnetic field after degradation of MB to obtain a leaching solution. The concentration of leached iron ions detected by ICP was 0.5 mg L^{-1}. An experiment in the homogeneous Fenton process was carried out using the same concentration of ferric ions that were leached from the catalyst. Under identical operating conditions, the decolorization efficiency of the homogeneous Fenton process after 40 min was significantly less than the 98% removal observed in the heterogeneous system. Therefore, the catalytic activity was primarily attributed to the MPCMS-500 catalyst and not the dissolved iron ions. When only NH_2OH and H_2O_2 were added into the MB solution, only a little MB was removed because of the free radicals formed by H_2O_2 in the presence of reduced reagent NH_2OH.[35] The generation of $^{\bullet}OH$ was mainly due to heterogeneous catalysis by MPCMS-500. These results all suggested that the porous carbon support played a positive role during MB removal, protected Fe_3O_4 nanoparticles from oxidation, and contributed to a synergistic effect in MB degradation due to its adsorption property.

The formation of $^{\bullet}OH$ during decomposition of H_2O_2 was detected by a photoluminescence (PL) technique using terephthalic acid (TA) as a probe molecule.[36] Typically, 20 mg of a certain kind of as-synthesized catalyst was dispersed in a 20 mL aqueous solution consisting of 5×10^{-4} mol L^{-1} TA and 2×10^{-3} mol L^{-1} NaOH. Subsequently, certain amounts of the H_2O_2 and NH_2OH solution were added. The reactions were performed under continuous stirring at 30 °C. Samples (5 mL) were removed at 5 min intervals using a magnet and used for fluorescence spectral measurements. PL spectra of generated 2-hydroxyterephthalic acid were acquired at 446 nm, following excitation at 325 nm. As seen in Figure S5 in the SI, the amount of $^{\bullet}OH$ produced on the MPCMS-500

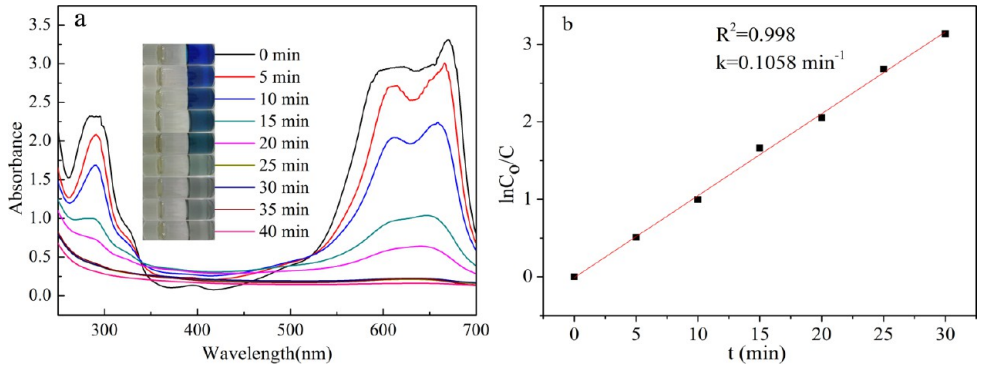

Figure 11. (a) UV−vis spectral changes of the 40 mg L^{-1} MB solution in the degradation process as a function of the reaction time in the presence of 2 g L^{-1} MPCMS-500, 4 mmol L^{-1} NH_2OH, and 16 mmol L^{-1} H_2O_2 at T = 303 K and pH 5.0. (b) First-order linear relationship.

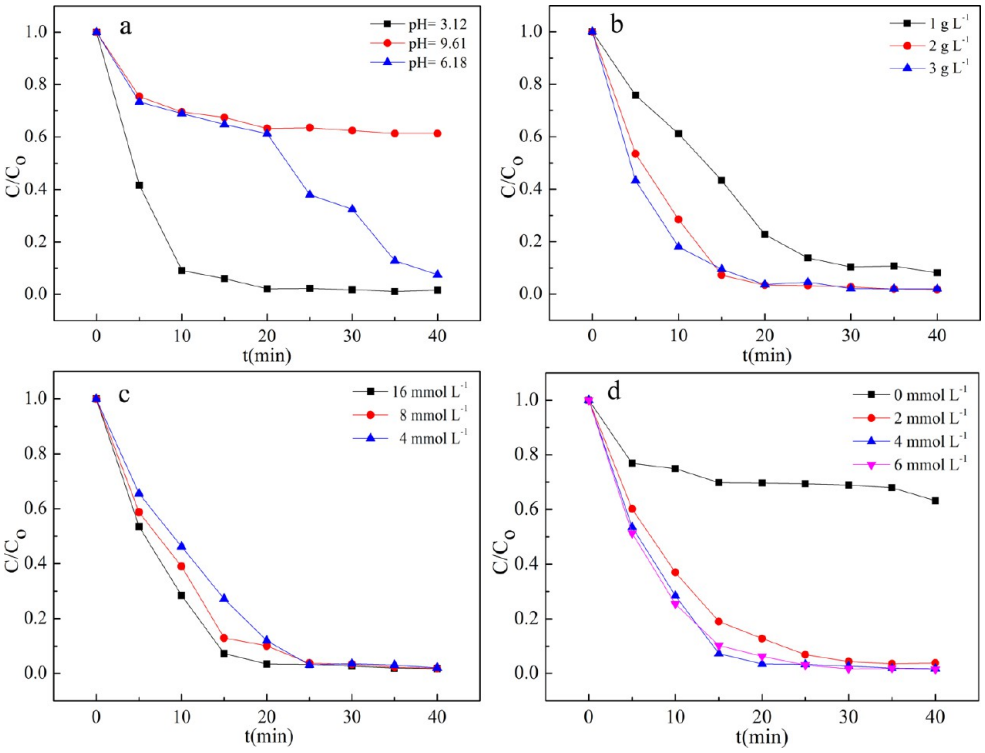

Figure 12. Effect of the (a) pH, (b) dosage of the catalyst, (c) H_2O_2 concentration, and (d) NH_2OH concentration on the removal of MB. Reaction conditions: (a) MB, 40 mg L^{-1}; H_2O_2, 4 mmol L^{-1}; NH_2OH, 4 mmol L^{-1}; MPCMS-500, 2 g L^{-1}; T = 303 K; (b) MB, 40 mg L^{-1}; H_2O_2, 16 mmol L^{-1}; NH_2OH, 4 mmol L^{-1}; pH 5.0; T = 303 K; (c) MB, 40 mg L^{-1}; NH_2OH, 4 mmol L^{-1}; MPCMS-500, 2 g L^{-1}; pH 5.0; T = 303 K; (d) MB, 40 mg L^{-1}; H_2O_2, 16 mmol L^{-1}; MPCMS-500, 2 g L^{-1}; pH 5.0; T = 303 K.

composite was greater than that of bare Fe_3O_4 at 5 min. These results were consistent with the higher degree of MB degradation for MPCMS-500 than for bare Fe_3O_4 and indicated that $^{\bullet}OH$ had a positive relationship with the catalytic activity for the degradation of MB in this study.

UV−vis spectra recorded during MB degradation (Figure 11a) exhibited bands at 465 and 292 nm that decreased rapidly and disappeared after 40 min of reaction, without the appearance of new adsorption bands in the visible or ultraviolet regions. This indicated that the benzene ring and hetero-polyaromatic linkages of MB were likely destroyed and MB was almost completely degraded. Electrospray ionization mass spectrometry (ESI-MS) was used to monitor the degradation of MB in the heterogeneous Fenton process. The ESI-MS spectrum obtained for the MB solution shows only a strong signal at m/z 284, which is related to the MB ion (Figure S6a in the SI). After 5 min of reaction with MPCMS-500 and H_2O_2, a new signal appears at m/z 300, as shown in Figure S6b in the SI. Figure S6c in the SI shows the ESI-MS spectrum for the reaction after 1 h. At this time, other m/z signals appear that are likely related to intermediates of the MB oxidation, also suggesting that the structural ring is somehow broken apart. The accompanying digital photographs of the MB solution revealed that the solution color gradually faded, consistent with the UV−vis spectra. In some cases, new peaks may appear in the UV−vis spectra, which indicate that MB is not totally degraded,[37−39] but no new peaks were observed in this current study. To better understand the reaction kinetics of MB degradation, the experimental data were fitted by a first-order model as expressed by eq 1, where C_0 and C are the initial and apparent concentrations of MB, respectively, and k is the

dx.doi.org/10.1021/am500576p | ACS Appl. Mater. Interfaces 2014, 6, 7275−7285

kinetic rate constant, which can be calculated from the slope of the straight line.

$$\ln(C_0/C) = kt \quad (1)$$

A first-order linear relationship was obtained, as seen in the plots of $\ln(C_0/C)$ versus reaction time (Figure 11b). The rate constant was calculated to be 0.1058 min^{-1}, which is much higher than the literature reported value of 0.1042 min^{-1} using Fe_3O_4@MIL-100(Fe) as the heterogeneous catalyst under ultraviolet-light irradiation,[40] and 2.35×10^{-3} min^{-1} reported using titanomagnetite as the catalyst at an H_2O_2 concentration of 300 mmol L^{-1}.[38]

3.3. Degradation under Different Conditions. *3.3.1. Effect of the Initial pH.* The removal of MB by carbon spheres in the presence of H_2O_2 and NH_2OH was investigated at pH values of 3.12, 9.61, and 6.18 (Figure 12a). It was observed that the degradation of MB was nearly 100% within 25 min at pH 3.12. The initial rate at pH 6.18 was relatively slow but later followed a faster degradation rate, and the removal efficiency then exceeded 90% within 40 min. At pH 9.61, the rate of reaction was slow and the conversion of MB was 38.7% over a period of 40 min. It is known that pH ≈3.0 is optimal for organic pollutant degradation by H_2O_2/iron in homogenous systems.[41] The optimum pH value for the decolorization of MB in this system was approximately 3, which can be seen in Figure 12a. This was in agreement with the classical Fenton reaction. However, unlike the conventional Fenton process, the removal efficiency achieved was 92.5% after 40 min of reaction, even when the initial pH was as high as 6.0. The degradation of MB is less efficient at higher pH because of the instability of H_2O_2 in an alkaline solution, and the production of $^{\bullet}OH$ on the surface of MPCMS-500 was gradually restricted with increasing pH, which also resulted in a slower degradation rate of MB.[5] The process of H_2O_2 activation by MPCMS is believed to involve the following steps. First, a complex is formed by ligand displacement between the hydrous surface of $\equiv Fe^{II}\cdot H_2O$ and H_2O_2, designated as $\equiv Fe^{II}\cdot H_2O_2$ (eq 2), where $\equiv Fe^{II}\cdot H_2O$ represents the α-Fe sites on the hydrous catalyst surface.[42−44] Then, the initially generated $\equiv Fe^{II}\cdot H_2O_2$ species produces $^{\bullet}OH$ by intramolecular electron transfer, leading to degradation and mineralization of MB (eqs 3 and 4).[4]

$$\equiv Fe^{II}\cdot H_2O + H_2O_2 \rightarrow \equiv Fe^{II}\cdot H_2O_2 \quad (2)$$

$$\equiv Fe^{II}\cdot H_2O_2 \rightarrow \equiv Fe^{III} + {}^{\bullet}OH + OH^- \quad (3)$$

$$^{\bullet}OH + MB \rightarrow CO_2 + H_2O \quad (4)$$

3.3.2. Effect of the Catalyst Dosage. The influence of the catalyst loading on the heterogeneous Fenton degradation of MB by MPCMS-500 was investigated using the catalyst at 1.0, 2.0, and 3.0 g L^{-1} (Figure 12b). The degradation efficiency increased from 85% to 98% as the catalyst concentration increased over the tested range. The increased efficiency, mainly due to increased catalyst loading, introduced more active sites, which allowed for greater production of free-radical species that promote the degradation reaction. A catalyst loading of 2 g L^{-1} led to MB being almost completely degraded within 20 min.

3.3.3. Effect of the H_2O_2 Concentration. Figure 12c illustrates the influence of the H_2O_2 concentration on the removal of MB dye using carbon spheres. The removal efficiency increased with increasing H_2O_2 concentration, reaching 97% even at a relatively low H_2O_2 concentration of 4 mmol L^{-1}. At lower concentrations, H_2O_2 could not generate a sufficient number of $^{\bullet}OH$ radicals, which slowed the oxidation rate and reduced the removal efficiency. Higher concentrations of H_2O_2 led to faster reactions as more radicals were formed. However, the advantages of higher concentrations are not unlimited, and there are two significant disadvantages of using high concentrations of H_2O_2. First, because of its overabundance relative to the pollutant, most of H_2O_2 would not have any substrate to act upon and would therefore be wasted. Second, higher H_2O_2 concentrations can lead to the scavenging of $^{\bullet}OH$ radicals[45] (eqs 5 and 6). Therefore, increasing the concentration of H_2O_2 beyond its optimal level would actually reduce the efficiency of the process.

$$H_2O_2 + {}^{\bullet}OH \rightarrow H_2O + {}^{\bullet}OOH \quad (5)$$

$$^{\bullet}OOH + {}^{\bullet}OH \rightarrow H_2O + O_2 \quad (6)$$

3.3.4. Effect of the NH_2OH Concentration. NH_2OH is a common reducing agent that is used to eliminate problems associated with a traditional homogenous Fenton system, such as the accumulation of Fe^{III} and the narrow pH range limits.[46] Research indicates that the presence of NH_2OH can accelerate the redox cycles of Fe^{III} to Fe^{II}. It can also alleviate Fe^{III} accumulation, enhance the reaction rates, and expand the effective pH range. In view of the excellent effects of NH_2OH in a homogenous Fenton system, we added it into the heterogeneous Fenton system to evaluate its synergistic effect in the degradation of MB in the presence of MPCMS-500 and H_2O_2. Data from the degradation of MB over a 2.0 g L^{-1} catalyst at pH 5.0 with different NH_2OH concentrations are summarized in Figure 12d. It was observed that the degradation percentage of MB increased from 36.8% to 98.5% when the NH_2OH concentration increased from 0 to 6 mmol L^{-1}. The degradation efficiency increased with increasing NH_2OH concentration. Even at low concentrations, the removal efficiency was above 90%. However, in a system with no NH_2OH, the degradation efficiency was low, and complete MB removal would likely require more time or higher H_2O_2 concentrations. According to the discussion above, the influence of NH_2OH on the degradation efficiency of MB on the surface of MPCMS was mainly attributed to the accelerated cycles of Fe^{2+} and Fe^{3+}. These results indicated that NH_2OH also produced a positive effect in the heterogeneous Fenton system.

3.4. Stability and Reuse of the Catalyst. To evaluate the stability of the catalysts, recycling reactions were carried out for the degradation of MB over MPCMS-500 in the presence of H_2O_2 and NH_2OH. In each test, the catalyst was separated from the solution using an external magnetic field, washed with ethanol, and vacuum-dried at 55 °C. As seen in Figure 13, the catalyst retained its original activity after 10 repeated reuses. Both of the MB and TOC concentrations were detected to evaluate the catalytic activity in the repeated process. The initial TOC concentration of a 40 mg L^{-1} MB solution was 20.36 mg L^{-1}. The results indicate that the efficiency of TOC removal was lower than the MB removal efficiency with each repetition, with a maximum for TOC removal at 68%, while that of MB removal was nearly 100%. These results indicated that MB was not totally mineralized, although the degraded products did not exhibit UV−vis spectral absorbances, as illustrated in Figure 11a. The eventual decrease of the catalytic activity may have been caused by the incomplete removal of byproducts during washing.[6] This may also have been due to small amounts of

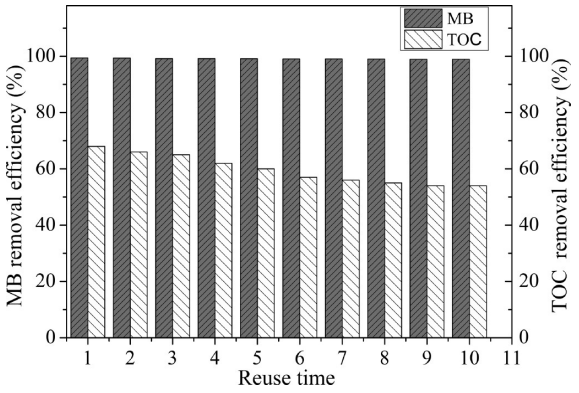

Figure 13. Reuse of the catalyst. Reaction conditions: initial MB concentration, 40 mg L^{-1}; initial H_2O_2 concentration, 16 mmol L^{-1}; NH_2OH concentration, 4 mmol L^{-1}; catalyst load, 2 g L^{-1}; pH 5.0; T = 303 K.

iron leaching from the surface of the catalyst during the degradation reactions.[47−49] The results also indicate that the stability of MPCMS-500 is very well compared with other heterogeneous Fenton catalysts;[6,50] there is almost no activity decrease of the catalyst after 10 repeated uses.

XPS was used to investigate the structure of the catalyst before and after the Fenton reaction. The details of the Fe 2p peaks (Fe $2p_{1/2}$ and Fe $2p_{3/2}$) of the MPCMS-500 samples before and after use during MB degradation are presented in Figure 14. The results indicate the presence of two oxidation states for the surface iron species. The Fe $2p_{3/2}$ peak of the catalyst can be deconvoluted into two components defined by peak positions at 710.0 and 711.6 eV, which correspond to the Fe^{2+} and Fe^{3+} ions, respectively.[51] The major component is found to be Fe^{3+}, which contributes 67.5% of the total iron surface atoms, while 32.5% of the total iron surface atoms are in the Fe^{2+} state. This result corresponds with the Fe_3O_4 crystal structure. The result also indicates the presence of a small amount of Fe_2O_3 in MPCMS-500, which is consistent with the XRD and MS characterization. For the sample after MB degradation, Fe^{3+} was found to be 71.3%. This indicated that part of Fe^{2+} in the outermost layer of the catalyst was oxidized into Fe^{3+} during the Fenton reaction. All of these results further indicated that the catalyst exhibited excellent durability because of the protective effects of the porous carbon support and the presence of NH_2OH.

4. CONCLUSIONS

Magnetic porous carbon spheres were fabricated by annealing, at 250 °C, the porous PS microspheres that had been sulfonated and loaded with Fe^{2+} by ion exchange. Subsequent annealing at 500 °C under an inert atmosphere produced particles that were used to catalyze the decolorization of the MB solution in a heterogeneous Fenton process in the presence of H_2O_2 and NH_2OH. The spheres were able to effectively catalyze the decomposition of H_2O_2 into radicals. The initial pH, catalyst dosage, and H_2O_2 and NH_2OH concentrations each greatly influenced the efficiency of MB degradation. The catalyst was shown to be stable and reusable, indicating that it could overcome the drawbacks of homogeneous catalysts. This study may aid in the further development of effective heterogeneous Fenton catalysts for the degradation of organic pollutants.

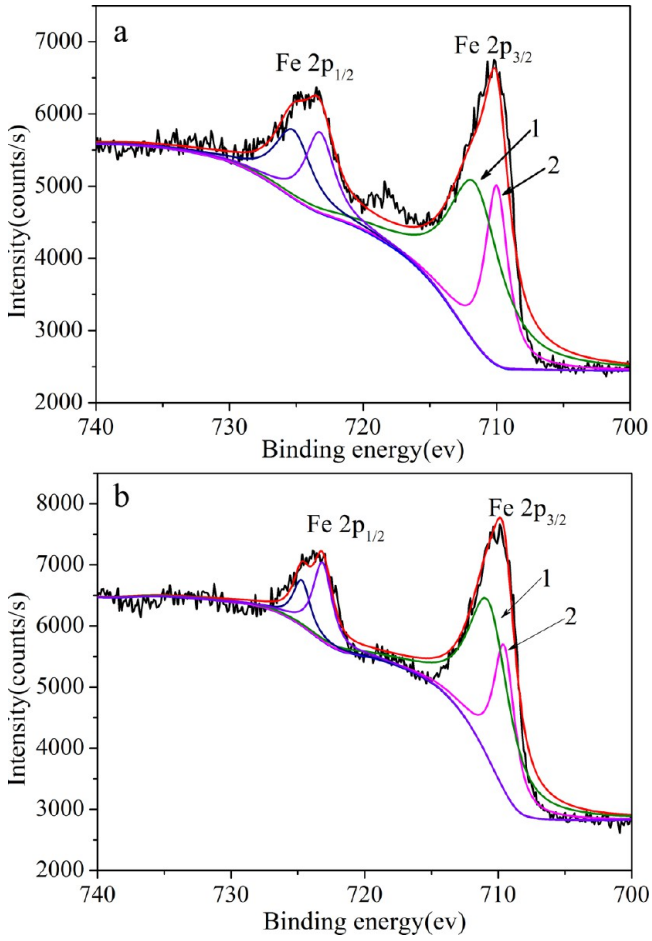

Figure 14. XPS spectrum of iron on MPCMS-500 before (a) and after (b) degradation of MB. Components 1 and 2 are due to the Fe^{3+} and Fe^{2+} species.

■ ASSOCIATED CONTENT

Ⓢ Supporting Information

SEM images of PS seed and porous PS, FT-IR spectra of porous PS and PS-SO_3H and of PS-250, MPCMS-500, and MPCMS-800, photographs of a MB solution before magnetic carbon microspheres was added, of a MB solution that was treated by magnetic carbon microspheres in the presence of H_2O_2 and NH_2OH, and of degradation and magnetic separation of MB by as-prepared magnetic carbon microspheres, fluorescence spectra of the various samples in a 5 × 10^{-4} mol L^{-1} NaOH solution of TA (excitation at 325 nm) at a fixed 5 min, ESI-MS spectra for monitoring the oxidation of MB at different reaction times, BET surface area, pore volume, and pore size of the PS, PS-250, MPCMS-500, and MPCMS-800 microspheres, and a summary of the BET surface areas of magnetic carbon microspheres that were fabricated by annealing polymer spheres reported previously and those investigated in the present work. This material is available free of charge via the Internet at http://pubs.acs.org.

■ AUTHOR INFORMATION

Corresponding Author

*Tel: 86-931-8912528. E-mail: zhoulc@lzu.edu.cn.

Notes

The authors declare no competing financial interest.

■ ACKNOWLEDGMENTS

The authors acknowledge financial support provided by the Fundamental Research Funds for the Central Universities (lzujbky-2013-65) and the National Science Foundation for Fostering Talents in Basic Research of the National Natural Science Foundation of China (Grant J1103307).

■ REFERENCES

(1) Neamu, M.; Catrinescu, C.; Kettrup, A. Effect of Dealumination of Iron(III)-Exchanged Y Zeolites on Oxidation of Reactive Yellow 84 Azo Dye in the Presence of Hydrogen Peroxide. *Appl. Catal., B* **2004**, *51*, 149−157.

(2) Pérez, M.; Torrades, F.; Domènech, X.; Peral, J. Fenton and Photo-Fenton Oxidation of Textile Effluents. *Water Res.* **2002**, *36*, 2703−2710.

(3) Salem, I. A. Kinetics of the Oxidative Color Removal and Degradation of Bromophenol Blue with Hydrogen Peroxide Catalyzed by Copper(II)-Supported Alumina and Zirconia. *Appl. Catal., B* **2000**, *28*, 153−162.

(4) Hu, X.; Liu, B.; Deng, Y.; Chen, H.; Luo, S.; Sun, C.; Yang, P.; Yang, S. Adsorption and Heterogeneous Fenton Degradation of 17α-methyltestosterone on Nano Fe_3O_4/MWCNTs in Aqueous Solution. *Appl. Catal., B* **2011**, *107*, 274−283.

(5) Ji, F.; Li, C.; Zhang, J.; Deng, L. Efficient Decolorization of Dye Pollutants with $LiFe(WO_4)_2$ as a Reusable Heterogeneous Fenton-like Catalyst. *Desalination* **2011**, *269*, 284−290.

(6) Nguyen, T. D.; Phan, N. H.; Do, M. H.; Ngo, K. T. Magnetic Fe_2MO_4 (M = Fe, Mn) Activated Carbons: Fabrication, Characterization and Heterogeneous Fenton Oxidation of Methyl Orange. *J. Hazard. Mater.* **2011**, *185*, 653−661.

(7) Wang, H.; Huang, Y. Prussian-blue-Modified Iron Oxide Magnetic Nanoparticles as Effective Peroxidase-like Catalysts to Degrade Methylene Blue with H_2O_2. *J. Hazard. Mater.* **2011**, *191*, 163−169.

(8) Zhang, S.; Zhao, X.; Niu, H.; Shi, Y.; Cai, Y.; Jiang, G. Superparamagnetic Fe_3O_4 Nanoparticles as Catalysts for the Catalytic Oxidation of Phenolic and Aniline Compounds. *J. Hazard. Mater.* **2009**, *167*, 560−566.

(9) Chun, J.; Lee, H.; Lee, S. H.; Hong, S. W.; Lee, J.; Lee, C. Magnetite/Mesocellular Carbon Foam as a Magnetically Recoverable Fenton Catalyst for Removal of Phenol and Arsenic. *Chemosphere* **2012**, *89*, 1230−1237.

(10) Hu, X.; Deng, Y.; Gao, Z.; Liu, B.; Sun, C. Transformation and Reduction of Androgenic Activity of 17α-methyltestosterone in Fe_3O_4/MWCNTs−H_2O_2 System. *Appl. Catal., B* **2012**, *127*, 167−174.

(11) Kong, L.; Lu, X.; Bian, X.; Zhang, W.; Wang, C. Constructing Carbon-Coated Fe_3O_4 Microspheres as Antiacid and Magnetic Support for Palladium Nanoparticles for Catalytic Applications. *ACS Appl. Mater. Interfaces* **2010**, *3*, 35−42.

(12) Liu, W.; Qian, J.; Wang, K.; Xu, H.; Jiang, D.; Liu, Q.; Yang, X.; Li, H. Magnetically Separable Fe_3O_4 Nanoparticles-Decorated Reduced Graphene Oxide Nanocomposite for Catalytic Wet Hydrogen Peroxide Oxidation. *J. Inorg. Organomet. Polym.* **2013**, *23* (4), 907−916.

(13) Guo, S.; Zhang, G.; Guo, Y.; Yu, J. C. Graphene Oxide−Fe_2O_3 Hybrid Material as Highly Efficient Heterogeneous Catalyst for Degradation of Organic Contaminants. *Carbon* **2013**, *60*, 437−444.

(14) Gu, L.; Zhu, N.; Guo, H.; Huang, S.; Lou, Z.; Yuan, H. Adsorption and Fenton-like Degradation of Naphthalene Dye Intermediate on Sewage Sludge Derived Porous Carbon. *J. Hazard. Mater.* **2013**, *246-247*, 145−153.

(15) Zhao, H.; Wang, Y.; Wang, Y.; Cao, T.; Zhao, G. Electro-Fenton Oxidation of Pesticides with a Novel Fe_3O_4@Fe_2O_3/Activated Carbon Aerogel Cathode: High Activity, Wide pH Range and Catalytic Mechanism. *Appl. Catal., B* **2012**, *125*, 120−127.

(16) Deng, J.; Wen, X.; Wang, Q. Solvothermal in Situ Synthesis of Fe_3O_4-Multi-Walled Carbon Nanotubes with Enhanced Heterogeneous Fenton-like Activity. *Mater. Res. Bull.* **2012**, *47*, 3369−3376.

(17) Amara, D.; Grinblat, J.; Margel, S. Synthesis of Magnetic Iron and Iron Oxide Micrometre-Sized Composite Particles of Narrow Size Distribution by Annealing Iron Salts Entrapped within Uniform Porous Poly(divinylbenzene) Microspheres. *J. Mater. Chem.* **2010**, *20*, 1899−1906.

(18) Amara, D.; Margel, S. Synthesis and Characterization of Superparamagnetic Core−Shell Micrometre-Sized Particles of Narrow Size Distribution by a Swelling Process. *J. Mater. Chem.* **2012**, *22*, 9268−9276.

(19) Snovski, R.; Grinblat, J.; Margel, S. Synthesis and Characterization of Magnetic Poly(divinylbenzene)/Fe_3O_4, C/Fe_3O_4/Fe, and C/Fe Onionlike Fullerene Micrometer-Sized Particles with a Narrow Size Distribution. *Langmuir* **2011**, *27*, 11071−11080.

(20) Amara, D.; Margel, S. Solventless Thermal Decomposition of Ferrocene as a New Approach for the Synthesis of Porous Superparamagnetic and Ferromagnetic Composite Microspheres of Narrow Size Distribution. *J. Mater. Chem.* **2011**, *21*, 15764−15772.

(21) Liu, Y.; Yan, H. Carbon Microspheres with Embedded Magnetic Iron Oxide Nanoparticles. *Mater. Lett.* **2011**, *65*, 1063−1065.

(22) Unsal, E.; Camli, S. T.; Senel, S.; Tuncel, A. Chromatographic Performance of Monodisperse−Macroporous Particles Produced by "Modified Seeded Polymerization". I: Effect of Monomer/Seed Latex Ratio. *J. Appl. Polym. Sci.* **2004**, *92*, 607−618.

(23) Wu, D.; Ge, X.; Zhang, Z.; Wang, M.; Zhang, S. Novel One-Step Route for Synthesizing CdS/Polystyrene Nanocomposite Hollow Spheres. *Langmuir* **2004**, *20*, 5192−5195.

(24) Zhang, Z.; Chalkova, E.; Fedkin, M.; Wang, C.; Lvov, S. N.; Komarneni, S.; Chung, T. C. M. Synthesis and Characterization of Poly(vinylidene fluoride)-*g*-sulfonated Polystyrene Graft Copolymers for Proton Exchange Membrane. *Macromolecules* **2008**, *41*, 9130−9139.

(25) Garcia, C.; Zhang, Y.; DiSalvo, F.; Wiesner, U. Mesoporous Aluminosilicate Materials with Superparamagnetic γ-Fe_2O_3 Particles Embedded in the Walls. *Angew. Chem., Int. Ed.* **2003**, *42*, 1526−1530.

(26) Zhang, W.; Wu, X.; Hu, J.; Guo, Y.; Wan, L. Carbon Coated Fe_3O_4 Nanospindles as a Superior Anode Material for Lithium-Ion Batteries. *Adv. Funct. Mater.* **2008**, *18*, 3941−3946.

(27) Cvelbar, U.; Chen, Z.; Sunkara, M. K.; Mozetic, M. Spontaneous Growth of Superstructure α-Fe_2O_3 Nanowire and Nanobelt Arrays in Reactive Oxygen Plasma. *Small* **2008**, *4*, 1610−1614.

(28) Fu, Y. Y.; Wang, R. M.; Xu, J.; Chen, J.; Yan, Y.; Narlikar, A. V.; Zhang, H. Synthesis of Large Arrays of Aligned α-Fe_2O_3 Nanowires. *Chem. Phys. Lett.* **2003**, *379*, 373−379.

(29) de Faria, D. L. A.; Venâncio Silva, S.; de Oliveira, M. T. Raman Microspectroscopy of Some Iron Oxides and Oxyhydroxides. *J. Raman Spectrosc.* **1997**, *28*, 873−878.

(30) Zhou, G.; Wang, D.; Li, F.; Zhang, L.; Li, N.; Wu, Z.; Wen, L.; Lu, G.; Cheng, H. Graphene-Wrapped Fe_3O_4 Anode Material with Improved Reversible Capacity and Cyclic Stability for Lithium Ion Batteries. *Chem. Mater.* **2010**, *22*, 5306−5313.

(31) Piao, Y.; Kim, H. S.; Sung, Y. E.; Hyeon, T. Facile Scalable Synthesis of Magnetite Nanocrystals Embedded in Carbon Matrix as Superior Anode Materials for Lithium-Ion Batteries. *Chem. Commun.* **2010**, *46*, 118−120.

(32) Lian, J.; Duan, X.; Ma, J.; Peng, P.; Kim, T.; Zheng, W. Hematite (α-Fe_2O_3) with Various Morphologies: Ionic Liquid-Assisted Synthesis, Formation Mechanism, and Properties. *ACS Nano* **2009**, *3*, 3749−3761.

(33) Ji, L.; Zhou, L.; Bai, X.; Shao, Y.; Zhao, G.; Qu, Y.; Wang, C.; Li, Y. Facile Synthesis of Multiwall Carbon Nanotubes/Iron Oxides for Removal of Tetrabromobisphenol A and Pb(II). *J. Mater. Chem.* **2012**, *22*, 15853−15862.

(34) Noorjahan, M.; Durga Kumari, V.; Subrahmanyam, M.; Panda, L. Immobilized Fe(III)-HY: an Efficient and Stable Photo-Fenton Catalyst. *Appl. Catal., B* **2005**, *57*, 291−298.

(35) Wang, S. Y.; Jiao, H. Scavenging Capacity of Berry Crops on Superoxide Radicals, Hydrogen Peroxide, Hydroxyl Radicals, and Singlet Oxygen. *J. Agric. Food. Chem.* **2000**, *48*, 5677−5684.

(36) Yu, J.; Wang, W.; Cheng, B.; Su, B. Enhancement of Photocatalytic Activity of Mesporous TiO_2 Powders by Hydrothermal Surface Fluorination Treatment. *J. Phys. Chem. C* **2009**, *113*, 6743−6750.
(37) Yang, S.; He, H.; Wu, D.; Chen, D.; Liang, X.; Qin, Z.; Fan, M.; Zhu, J.; Yuan, P. Decolorization of Methylene Blue by Heterogeneous Fenton Reaction Using $Fe_{3-x}Ti_xO_4$ ($0 \leq x \leq 0.78$) at Neutral pH Values. *Appl. Catal., B* **2009**, *89*, 527−535.
(38) Yang, S.; He, H.; Wu, D.; Chen, D.; Ma, Y.; Li, X.; Zhu, J.; Yuan, P. Degradation of Methylene Blue by Heterogeneous Fenton Reaction Using Titanomagnetite at Neutral pH Values: Process and Affecting Factors. *Ind. Eng. Chem. Res.* **2009**, *48*, 9915−9921.
(39) Ibrahim, A. M. A.; Al-Ashqar, S. M. A. Spectroscopic and Kinetic Studies on the Degradation of Methylene Blue Using the Supramolecular Coordination Polymer $[(Ph_3Sn)_4Fe(CN)_6]$ as Catalyst. *Spectrochim. Acta, Part A* **2012**, *92*, 238−244.
(40) Zhang, C.; Qiu, L.; Ke, F.; Zhu, Y.; Yuan, Y.; Xu, G.; Jiang, X. A Novel Magnetic Recyclable Photocatalyst Based on a Core−Shell Metal−Organic Framework Fe_3O_4@MIL-100(Fe) for the Decolorization of Methylene Blue Dye. *J. Mater. Chem. A* **2013**, *1*, 14329−14334.
(41) Arnold, S. M.; Hickey, W. J.; Harris, R. F. Degradation of Atrazine by Fenton's Reagent: Condition Optimization and Product Quantification. *Environ. Sci. Technol.* **1995**, *29*, 2083−2089.
(42) Luo, W.; Zhu, L.; Wang, N.; Tang, H.; Cao, M.; She, Y. Efficient Removal of Organic Pollutants with Magnetic Nanoscaled $BiFeO_3$ as a Reusable Heterogeneous Fenton-Like Catalyst. *Environ. Sci. Technol.* **2010**, *44*, 1786−1791.
(43) Pham, A. L.; Lee, C.; Doyle, F. M.; Sedlak, D. L. A Silica-Supported Iron Oxide Catalyst Capable of Activating Hydrogen Peroxide at Neutral pH Values. *Environ. Sci. Technol.* **2009**, *43*, 8930−8935.
(44) Lin, S.; Gurol, M. D. Catalytic Decomposition of Hydrogen Peroxide on Iron Oxide: Kinetics, Mechanism, and Implications. *Environ. Sci. Technol.* **1998**, *32*, 1417−1423.
(45) Xue, X.; Hanna, K.; Abdelmoula, M.; Deng, N. Adsorption and Oxidation of PCP on the Surface of Magnetite: Kinetic Experiments and Spectroscopic Investigations. *Appl. Catal., B* **2009**, *89*, 432−440.
(46) Chen, L.; Ma, J.; Li, X.; Zhang, J.; Fang, J.; Guan, Y.; Xie, P. Strong Enhancement on Fenton Oxidation by Addition of Hydroxylamine to Accelerate the Ferric and Ferrous Iron Cycles. *Environ. Sci. Technol.* **2011**, *45*, 3925−3930.
(47) Deng, J.; Jiang, J.; Zhang, Y.; Lin, X.; Du, C.; Xiong, Y. $FeVO_4$ as a Highly Active Heterogeneous Fenton-like Catalyst Towards the Degradation of Orange II. *Appl. Catal., B* **2008**, *84*, 468−473.
(48) Ramirez, J. H.; Costa, C. A.; Madeira, L. M.; Mata, G.; Vicente, M. A.; Rojas-Cervantes, M. L.; López-Peinado, A. J.; Martín-Aranda, R. M. Fenton-like Oxidation of Orange II Solutions Using Heterogeneous Catalysts Based on Saponite Clay. *Appl. Catal., B* **2007**, *71*, 44−56.
(49) Tekbaş, M.; Yatmaz, H. C.; Bektaş, N. Heterogeneous Photo-Fenton Oxidation of Reactive Azo Dye Solutions Using Iron Exchanged Zeolite as a Catalyst. *Microporous Mesoporous Mater.* **2008**, *115*, 594−602.
(50) Zhu, M.; Diao, G. Synthesis of Porous Fe_3O_4 Nanospheres and Its Application for the Catalytic Degradation of Xylenol Orange. *J. Phys. Chem. C* **2011**, *115*, 18923−18934.
(51) Dhananjeyan, M. R.; Mielczarski, E.; Thampi, K. R.; Buffat, P.; Bensimon, M.; Kulik, A.; Mielczarski, J.; Kiwi, J. Photodynamics and Surface Characterization of TiO_2 and Fe_2O_3 Photocatalysts Immobilized on Modified Polyethylene Films. *J. Phys. Chem. B* **2001**, *105*, 12046−12055.